Multi-Channel Photonic Crystal Fiber Based Surface Plasmon Resonance Sensor for Multi-Analyte Sensing
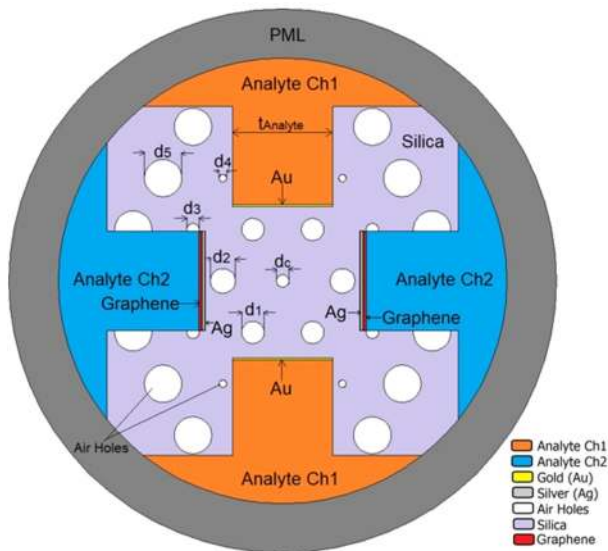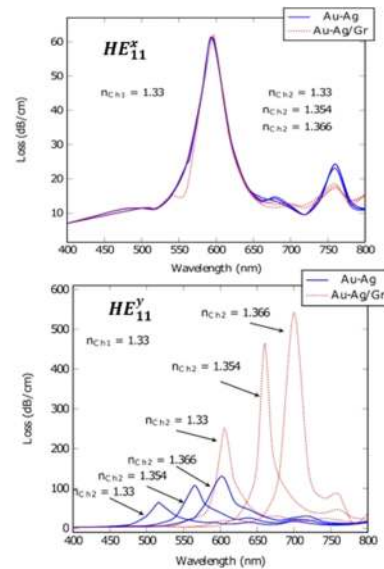
Ahmet Yasli
Huseyin Ademgil, *Senior Member, IEEE*
Shyqyri Haxha, *Senior Member, IEEE*
Amar Aggoun, *Senior Member, IEEE*

Multi-Channel PCF based SPR Sensor with Graphene Protecting Silver Layer for Multi-Analyte Sensing.

Loss variation as a function of wavelength for HE_{11}^x and HE_{11}^y fundamental modes

Multi-Channel Photonic Crystal Fiber Based Surface Plasmon Resonance Sensor for Multi-Analyte Sensing

Ahmet Yasli [ID],[1] **Huseyin Ademgil** [ID],[2] *Senior Member, IEEE*,
Shyqyri Haxha [ID],[3] *Senior Member, IEEE*,
and Amar Aggoun,[4] *Senior Member, IEEE*

[1] Department of Electrical and Electronics Engineering, European University of Lefke,
TR-10 Mersin, Turkey
[2] Department of Computer Engineering, European University of Lefke, TR-10 Mersin, Turkey
[3] Department of Electronic Engineering, School of Engineering, Physical and Mathematical
Sciences, Royal Holloway, University of London, Egham TW20 0EX, U.K.
[4] School of Mathematics and Computer Science, University of Wolverhampton,
Wolverhampton WV1 1LY, U.K.

Abstract: In this paper, we report a unique multi-channel Photonic Crystal Fibre (PCF) sensor based on Surface Plasmon Resonance (SPR) structure comprising of silver and gold doped plasmonic layers for multi-analyte sensing applications. We deployed a Full Vectorial Finite Element Method (FV-FEM) to investigate the sensitivity performance of the proposed PCF sensor. The SPR sensor is fully optimised to ensure propagation features, such as confinement loss, resonance condition, resolution and sensitivity are investigated within various optimised design parameters. According to spectral sensitivity analyses, 2500 nm/RIU and 3083 nm/RIU with 4×10^{-5} RIU and 3.2×10^{-5} RIU resolutions are obtained for Channel 1 (Ch1) (x-polarized) and Channel 2 (Ch2) (y-polarized), respectively.

Index Terms: Photonic crystal fiber (PCF), surface plasmon resonance (SPR), multi analyte, multi channel, fiber optic sensor.

1. Introduction

Surface Plasmon Resonance (SPR) method is one of the proven advanced techniques used for detecting molecular interaction. The SPR method can be applied to various sensing applications such as chemical [1], biochemical [2] and bio-sensing [3] without molecule labelling requirements [4]. Kretschmann Raether prism geometry [5], optical fibre coupling [6]–[9] and diffraction on periodic metallic gratings [10], [11] are the most known approaches, whereby SPR techniques can be applied. When comparing the stated approaches [1]–[11], optical fibre based techniques can offer extra additional advantages [12]. Particularly, when the SPR method is combined with the Photonic Crystal Fibre (PCF) technology, they become very attractive for designing sensors with high sensitivity and selectivity. As know, unique propagation and physical properties of the PCFs offer significant advantages in terms of designing fibre sensors with high sensitivity and selectivity performance.

The advantages of PCF sensor devices such as; lightweight, compactness and high signal-to-noise ratio, allows these devices to be very attractive for designing high rate-robust sensors for various sensing applications. Furthermore, their electromagnetic interference resistivity and remote sensing abilities make them amongst the best alternative sensor devices when compared against other bulky sensor configuration approaches [13], [6].

The SPR based sensors, reported by Kretschmann Raether prism geometry [5], relies on detecting the Refractive Index (RI) changes on the target medium. The RI change follows when the resonance condition transpires. The resonance condition phenomenon can be simply described as the phase matching of p-polarized light and the Surface Plasmon Waves (SPW) onplasmonic surfaces. During the resonance condition, the optimum energy transfer from fundamental mode to plasmons occurs where the highest confinement loss level is reached. In this regard, the resonance wavelength variations are indicating within the RI changes of the targeted medium. The spectral interrogation method is used to sense the variations of resonance wavelengths (peak points) [14]. However, due to the high cost and bulky configuration of Kretschmann Raether's prism geometry, optical fibre based sensors are deemed more suitable for remote sensing and miniaturized sensor applications [1]. Previously published articles shown that special type structures such as U-shaped [15], [16] and D- shaped [17] PCF based SPR models exhibits high sensitivity for various analytes. Moreover, exceptional optical properties of PCFs, including high filtering performance [18], ultra-low confinement loss and large effective mode area [19], large cut-off ratio for endlessly single-mode propagation [20], low bending loss [21], rich double-cladding features [22], composite resonant cavity [23] high-birefringent [24], ultra-flat dispersion [25] may provide additional advantages on designing a sensor with desired propagation features. To the best of our knowledge, Hassani *et al*. [6] initially combined the PCF technology with the SPR method. This phenomenon took SPR based sensors one step forward when comparing with previous sensor structures [6]. This work [6] involved two different designs, where the analyte channel was covered internally and externally by a metallic layer. Since then, many similar sensor designs for single analyte sensing purposes have been reported [14], [24], [26]–[29]. On the other hand, reducing the sensing time and possibility of simultaneous sensing of multi targets became visible by using a multi-analyte sensing approach. In 2011, Zhang *et al*. [30] proposed the first Micro-structured Optical Fiber (MOF) based multichannel plasmonic sensor design for multi-analyte sensing. In this study [30], to overcome the sample infiltration challenge of micron-sized channels, wagon wheel fibre with gold as a plasmonic material is used. Theoretically, 1535 nm/RIU and 1550 nm/RIU sensitivity levels are reported for Channel 1 (Ch1) and Channel 2 (Ch2), respectively, where the RI varies between 1.33 and 1.46.

In 2015, Otupuri *et al*. [31] demonstrated a PCF based multi-analyte sensor, where Au and Ta_2TO_5 are used as an active plasmonic material between large micro-fluidic analyte channels and cladding of the PCF core. High birefringence is achieved by employing the elliptical air holes in the cladding region. In this study [31], the reported sensitivity levels were up to 4600 nm/RIU for Ch1 (x-polarized) and 2300 nm/RIU for Ch2 (y-polarized) where RI varies between 1.33 to 1.36. Following year, Azzam *et al*. [32] have numerically investigated a similar multi-analyte sensor structure. In this study [32], resonance conditions of higher-order modes are investigated, where Au was engaged as plasmonic material. It is found that sensitivity levels of 2200, 2400, 2200, and 2400 nm/RIU can be reached with the HE_{11}^x, HE_{11}^y, HE_{21}^x and HE_{21}^y, respectively. On the other hand, Lu *et al*. [33] demonstrated a dual-channel multilayer-coated SPR sensor for dual refractive index measurements. In this study, a conventional optical fibre structure is used with externally coated bilayer (Au with Indium Tin Oxide (ITO)) and internally coated with Ag layers. in Ref. [33] have numerically calculated that 1951 nm/RIU and 2496 nm/RIU sensitivities can be achieved for Ch1 and Ch2, respectively. Recently, Kaur *et al*. [34] demonstrated also a multi-analyte SPR sensor based on PCF structure. In their design [34], dual analyte channels surrounded by Au layers in the core region of the PCF are proposed, where the RI of analyte varies between 1.30–1.40. They [34] have achieved sensitivity levels of 1000 nm/RIU and 3750 nm/RIU for Ch1 and Ch2, respectively.

Previous research has shown that multi-analyte optical sensors; exhibit unique features that can be applied in various sensing applications [14]–[24]. In our proposed structure, to achieve desired propagation features a new PCF structure configuration is designed and optimised. It is well known
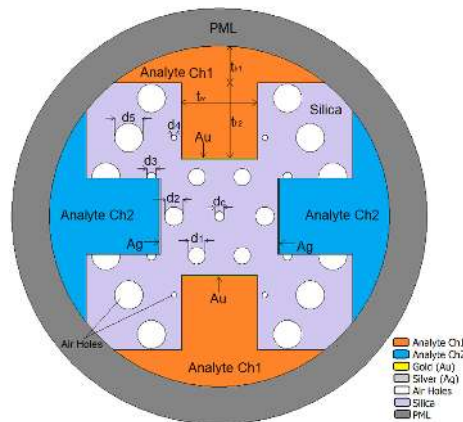
Fig. 1. Cross section of proposed PCF-SPR sensors.

that, sought after propagation features; such as resonance wavelength, confinement loss and birefringence can be controlled by tuning the design parameters of PCF structure. Therefore, PCF design parameters such as hole-to-hole distance, air hole size and air hole shape are significant. Additionally, the sensor channels where the analyte is investigated; the channel size, channel distance and thickness of the metallic layers play a critical role in achieving such desired propagation features. These aforementioned parameters are crucial for the practical implementation of the proposed sensor. As a result, large analyte channels with outer metal layer designs [6], [28] and the considerably large hole-to-hole spacing would be a more practical solution. In addition to this, the study of the silver/gold was preferred as a metallic layer. In this proposed study, we demonstrate numerically external coated multi-channel PCF based SPR sensor, illustrated in Fig. 1. The proposed sensor is relying on four concentric channels for liquid analysis (Water (n = 1.33), Ethanol (n = 1.354) and several commercial hydrocarbon mixtures (n = 1.366) [35]). Due to the asymmetric nature of the proposed structure, x- and y- polarized modes are used individually for detecting analytes.

2. Modelling and Numerical Analysis

The highly sensitive proposed dual analyte PCF based SPR sensors configuration with four identical analyte channels is illustrated in Fig. 1. Full-Vectorial Finite Element Method (FV-FEM) is used to design, optimise and evaluate the sensor performance. Intensive simulations using FV-FEM have been performed for the stated analytes, and optimal structural parameters have been determined in terms of sensor sensitivity and selectivity.

Fig. 1 illustrates the cross section of proposed PCF-SPR sensors incorporating twenty-seven various sized air holes, which are hexagonally arranged on a silica background. As can be seen, circular-shaped Perfectly Matched Layers (PMLs) are employed around the sensor boundaries [25], [26]. The metal layers are placed on the face of four analyte channels towards the centre of the PCF core. To confine and guide the fundamental modes in the core region; various sized air holes (d_c, d_1, d_2, d_3, d_4, d_5) are located on the first, second and third ring of the proposed model. The phase-matching condition between the plasmon and fundamental core mode is controlled by varying the central air hole (d_c). The air holes, in the first ring (d_1, d_2), are designed to trap the light in the core region. On the other hand, the air holes in the second (d_3, d_4) and third (d_5) rings are used for tuning the amount of light leakage towards the outer shell of the PCF. The diameter of air holes are fixed as $d_c = 0.5$ μm, $d_1 = 0.9$ μm, $d_2 = 1$ μm, $d_3 = 0.5$ μm, $d_4 = 0.3$ μm and $d_5 = 1.5$ μm, while hole to hole distance (Λ) is set to 2.4 μm. The idea of utilizing diverse size air gaps in the cladding is to produce the birefringence, where it leads to divergent wavelength and SPR intensities of x- and y- polarized modes [14].

As can be seen from Fig. 1, four analyte channels are positioned perpendicular to each other. Vertically positioned identical channels hosting single analyte are labelled as Channel 1 (Ch1), while the horizontally positioned ones are accommodating different analyte are labelled as Channel 2 (Ch2). The analyte channels are constructed by etching the PCF from its edges towards the core. The etching width (t_w) is set be 4 μm, where the etching height is divided into two layers, the first layer (t_{h1}) is 2 μm and second one (t_{h2})) is 4 μm. The metal layer thicknesses are also set to 40 nm for both gold and silver. The gold and the silver permittivity values are wavelength depended, they are taken from Johnson and Christy [36] data, and Palik [37] data, respectively.

Next, we focus on finding the differences of confinement loss peaks (resonance condition) using the spectral sensitivity method. The loss curve is expected to reach the highest point at the resonance phase matching between core and plasmon modes. The confinement losses are calculated by using the equation [38], [39]:

$$\frac{40\pi}{\ln(10)\lambda} \text{Im}(n_{eff}) \times 10^4 \, [dB/cm] \tag{1}$$

where, Im(n_{eff}) is the imaginary part of effective refractive index.

The RI changes can be detected by varying analyte properties. The analyte variations can be realised with the shifts on resonance condition wavelength. The Resonance condition changes are directly affecting the propagation features of the fundamental mode, surface plasmon mode and the penetration depth of the evanescent field. The magnitude and wavelength shifts on the resonance condition (phase matching) are the main indications [40]. The sensitivity of these type of SPR sensors can be directly associated with resonance wavelength and the loss characteristics of the structure [41]. The spectral interrogation method is used to determine the sensitivity of the proposed PCF model at a particular operating wavelength. Differences of the phase-matching loss peaks are considered thoroughly and the following equation is used to calculate the sensitivity of the proposed SPR sensor [38]:

$$S(\lambda) = \frac{\Delta\lambda_{peak}}{\Delta\lambda_{na}} \quad (nm/RIU) \tag{2}$$

where, $\Delta\lambda_{peak}$ and Δn_a are differences of phase matching loss peaks and analyte RI, respectively.

The sensitivity and resolution levels of the SPR sensor are two critical parameters that determine the performance of SPR type sensors. Resolution (R) is defined as the minor variation detection of the resonance wavelength. The detection of SPR based sensors can be limited with the unbalanced sensitivity to resolution ratio. In this respect, high sensitivity with low resolution is desirable for these type of sensors [41]. Resolution (R) can be calculated using the following equation [38]:

$$R = \Delta_{na} \frac{\Delta\lambda_{min}}{\Delta\lambda_{peak}} \quad (RIU^{-1}) \tag{3}$$

where $\Delta\lambda_{min}$ is assumed to be 0.1 nm.

3. Results and Discussion

The resonance condition is the key parameter that affects the sensitivity performance of the proposed PCF sensor. It can be described as the maximum energy transfer from the reflected light into SPWs at the evanescent field. Due to this phenomenon, the confinement loss reaches its highest peak point at that particular wavelength. When the RI of analyte changes, the wavelength that satisfies the resonance condition also changes. To increase the interaction between the analyte and the sensing interactions, the stronger modal field is required [28]. Therefore, in this study, only the fundamental core (HE_{11}^x and HE_{11}^y) and plasmon modes are considered. The analyses that have been investigated, using the proposed PCF SPR sensor, are carried out in the x-y plane, while the incident light wave propagates in the z-direction.

The resonance condition for both HE_{11}^x and HE_{11}^y modes can be seen in Fig. 2(a) and Fig. 2(b), respectively. Fig. 2(a), illustrates the obtained results when the refractive index of analyte in Ch1 is
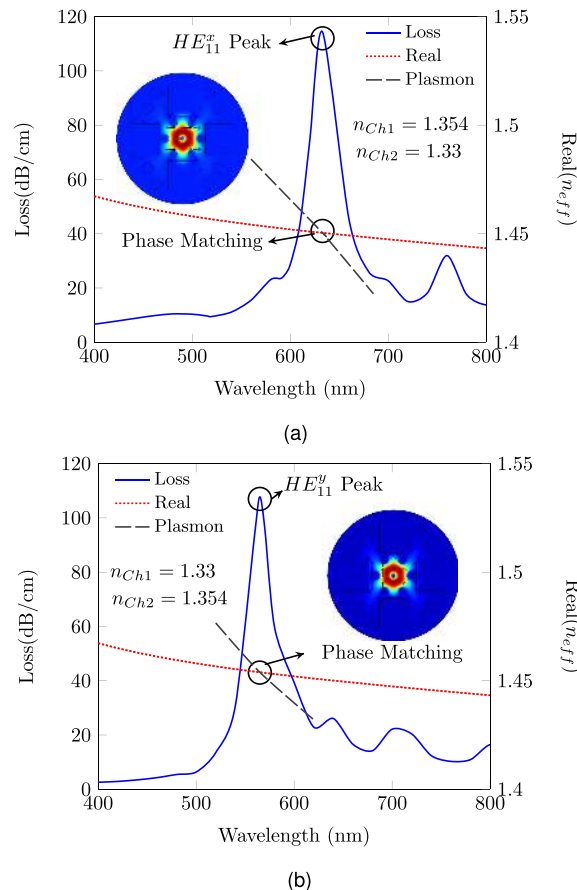
(a)

(b)

Fig. 2. Effective index distribution of fundamental core and plasmon modes as a function of loss at the phase matching point; (a) HE_{11}^x and (b) HE_{11}^y.

1.354 and in Ch2 is 1.33. Conversely, in Fig. 2(b), the analyte channel RI are exchanged with each other, where Ch1 is 1.33 and Ch2 is 1.354. It can be seen that x- and y- polarized fundamental (red dashed line) and plasmon (grey long dashed line) modes are intersecting at the operating wavelength 633 nm and 565 nm, respectively. Also, the highest peak points of loss curves are obtained at the same wavelength when plasmon and fundamental modes are interacting. At these peaks the maximum energy transform occurs from the core to the plasmon modes. In this study, two different (analyte) channels are used for simultaneous sensing of the proposed analytes. To investigate the performance of the proposed sensor, variations of RI in both channels have been tested. Initially, the RI value of Ch1 is fixed to 1.33, where 3 different analyte variations on Ch2 have been applied.

In Fig. 3(a) and (b), we illustrated the obtained results of the loss variation as a function of wavelength when Ch1 RI is fixed to 1.33; (a) HE_{11}^x and (b) HE_{11}^y. As can be seen from Fig. 3(a), the peak point of loss curves (resonance wavelengths) for x-polarized fundamental modes are not affected by analyte changes in Ch2. On the other hand, as can be seen from Fig. 3, resonance wavelength shifts to longer wavelengths and the loss levels are growing with RI increase for the y-polarized fundamental mode.

In Fig. 4, the contrary scenario is studied, where the RI value of Ch2 is fixed to 1.33. It can be seen that the resonance wavelength in x-polarized fundamental mode shifts to longer wavelengths with analyte variations, where no change has been observed in y-polarized mode. This shows that Ch1 is responding for x- polarized fundamental mode and Ch2 for y- polarized fundamental mode only. Therefore, this feature leads to simultaneous multi-analyte sensing.
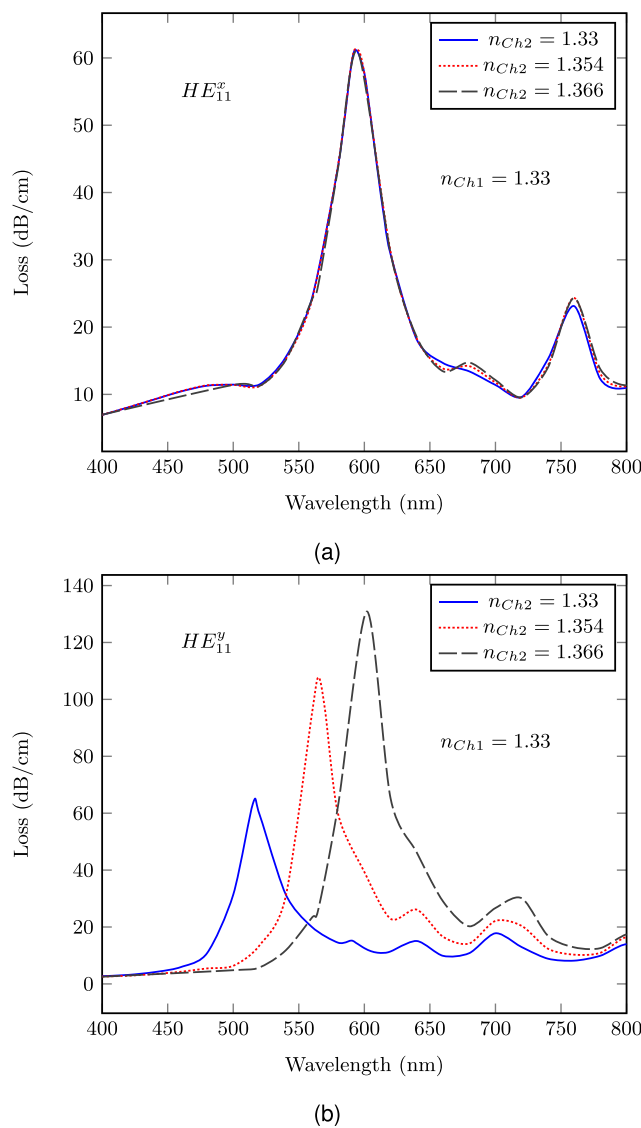
Fig. 3. Loss variation as a function of wavelength when Ch1 RI is fixed to 1.33; (a) HE_{11}^x and (b) HE_{11}^y.

Variation losses as a function of wavelength for both channels where the RI is fixed to 1.354 and 1.366 are validated in Fig. 5(a) and (c) for HE_{11}^x polarised; (b) and (d) for HE_{11}^y polarised, and Fig. 6(a) and (c) for HE_{11}^x polarised; (b) and (d) for HE_{11}^y polarised, respectively. Both figures have shown that the resonance wavelength behaviour of the proposed PCF sensor is experiencing similar trends to Fig. 3 and Fig. 4. Thus, if analyte RI in Ch1 kept constant while in Ch2 RI is varied, the changes on-resonance condition occurs only at y-polarized modes. Likewise, when analyte RI in Ch2 is kept constant while in Ch1 RI is varied, the changes on-resonance condition occurs only at x-polarized modes. The polarization mode response changes due to analyte RI changes, confirming that our proposed PCF based on SPR sensor can be used for multi-analyte sensing.

Previous studies have confirmed that silver is weak against oxidation [42]–[44]. Therefore, the requirement for an additional protection layer becomes vital for long-term sensor applications. In this regard, from a practical point of view, effects of the graphene as a protection layer are investigated. Schematics of the new PCF based SPR sensor configuration, when graphene is deployed as a protection layer for silver and gold, is illustrated in Fig. 7(a). Loss variation as a
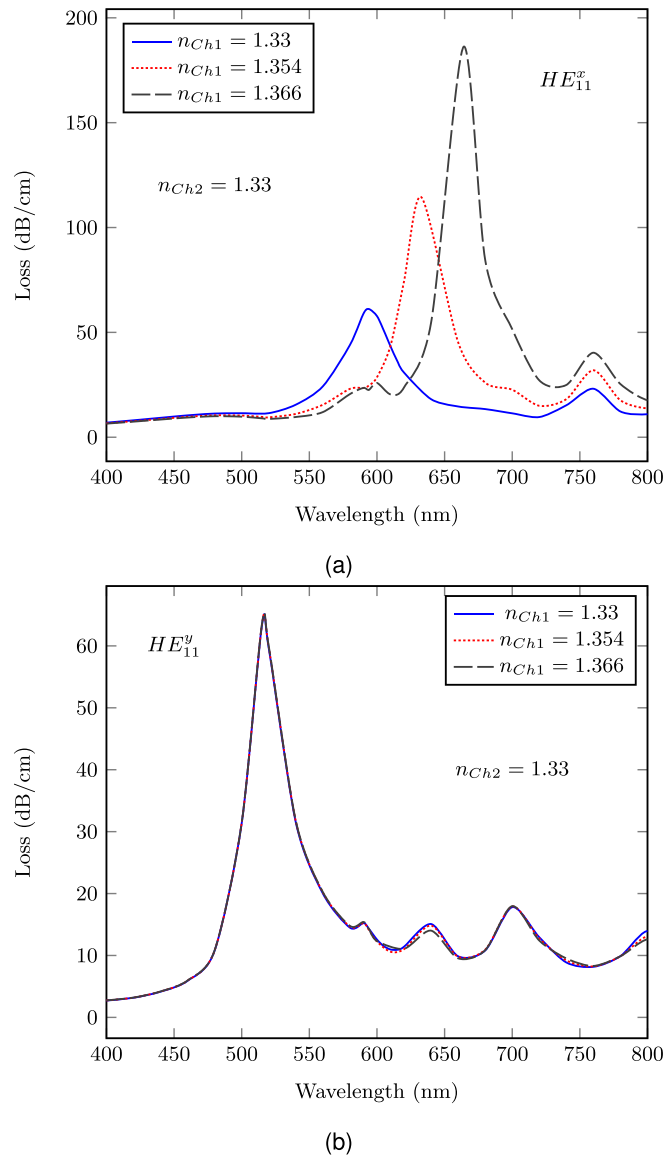
(a)

(b)

Fig. 4. Loss against wavelength when Ch2 RI is fixed to 1.33; (a) HE_{11}^x and (b) HE_{11}^y.

function of wavelength when Ch1 RI is fixed to 1.33 and Ch2 RI is varied (1.33, 1.354 and 1.366), are shown in Fig. 7(b) for HE_{11}^x and (c) HE_{11}^y, respectively It can be seen that when additional graphene layers are used, the sensor shows similar behaviour with Au-Ag layered structures. However, the level of loss peak curves on the y-polarized mode is increasing with the additional graphene layer. Due to the aromatic structure of the graphene layer, millions of benzene rings make the sensor surface much suitable for π-π stacking. This feature leads the sensor to interact with molecules in aromatic groups effectively. As a result of this interaction, the overall sensitivity of the sensor is enhanced in y- polarized mode. This change occurs only in the y-polarized mode due to the placement of silver and graphene layers.

Another critical factor that affects the propagation and interaction properties of the proposed PCF structure, is the size of the air holes within the cladding region. In terms of light confinement, larger air holes are desirable, however, this may limit the light leakage towards the metallic layers. Therefore, this would reduce the energy transfer from fundamental modes to surface plasmon

(a) Ch1 RI fixed to 1.354 for HE_{11}^x

(b) Ch1 RI fixed to 1.354 for HE_{11}^y

(c) Ch2 RI fixed to 1.354 for HE_{11}^x

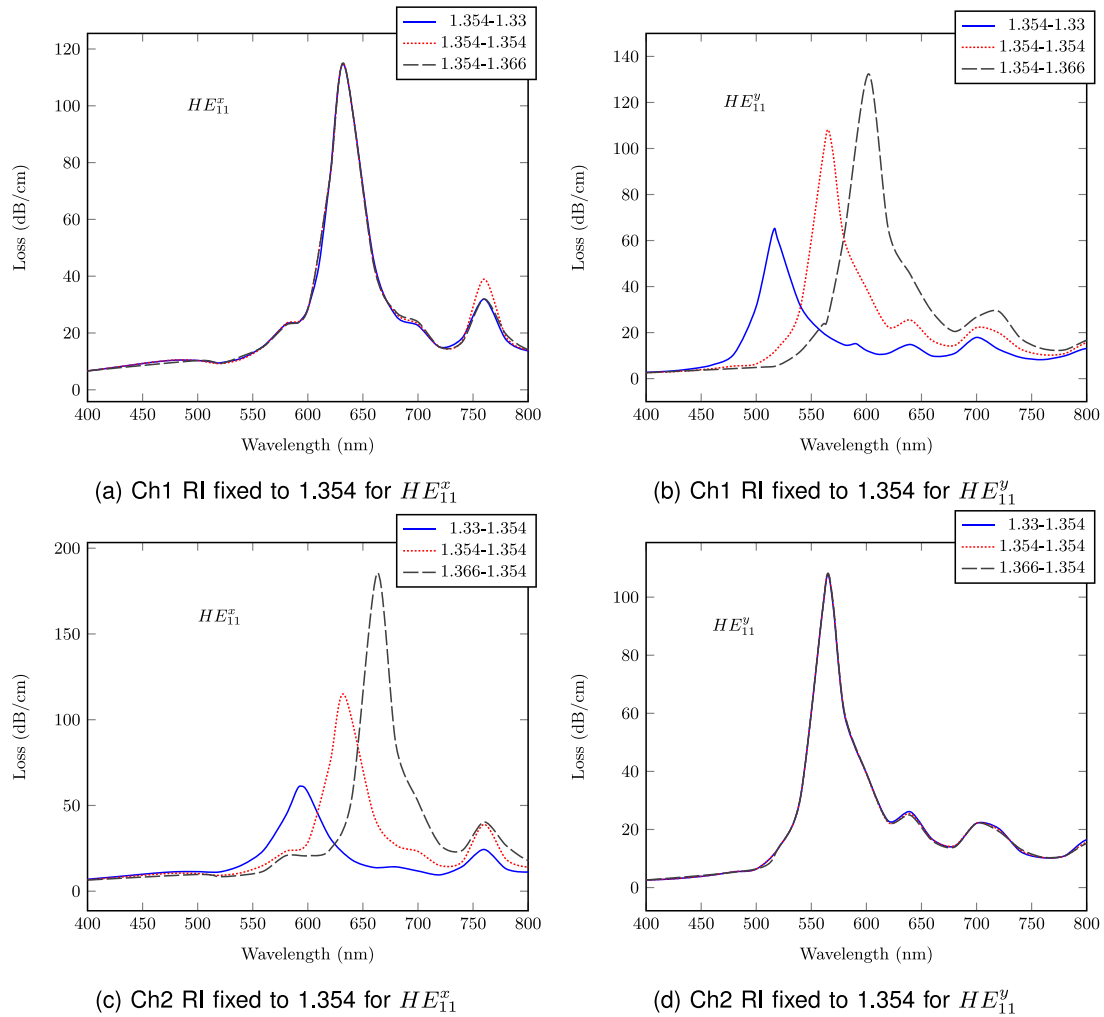(d) Ch2 RI fixed to 1.354 for HE_{11}^y

Fig. 5. Loss variation as a function of wavelength (when RI fixed to 1.354) for both Ch1 and Ch 2.

waves. On the other hand, smaller air holes may increase the light leakage towards the outer shell, however confinement loss will be too high may limit the sensor length, which would reduce the detection performance [6], [29]. Therefore, optimisation of precision dimensions of the size of air holes is critical.

In Fig. 8, the effect of the air hole sizes (d_1 and d_2) are investigated for both x- and y- polarized modes. As can be seen from both Fig. 7(a) and (b), the size of the air holes is determining the level of the losses. As expected, larger air hole sizes contribute to the reduction of losses, whereas the smaller size of air holes contribute to increasing the losses. Although there is immense change on the losses, 20% air hole size variation is not effecting the phase matching wavelengths.

The thickness of the metallic layer is another important factor that effects the interaction properties of the resonance condition of the proposed sensor structure. In Fig. 9, the effects of metal layer thicknesses from 30 nm to 50 nm are studied thoroughly for both polarised modes (a) HE_{11}^x and (b) HE_{11}^y. To make a fair comparison, the RI value is kept fixed to 1.33 for both analyte channels. It can be seen that the thicknesses of the metallic layer are decisive on the impact of the resonance condition. Thus, increasing metallic layer thickness lead to reduction of the loss levels, when the resonance condition is shifted to longer wavelengths.

(a) Ch1 RI is fixed to 1.366 for HE_{11}^x

(b) Ch1 RI fixed to 1.366 for HE_{11}^y

(c) Ch2 RI fixed to 1.366 for HE_{11}^x

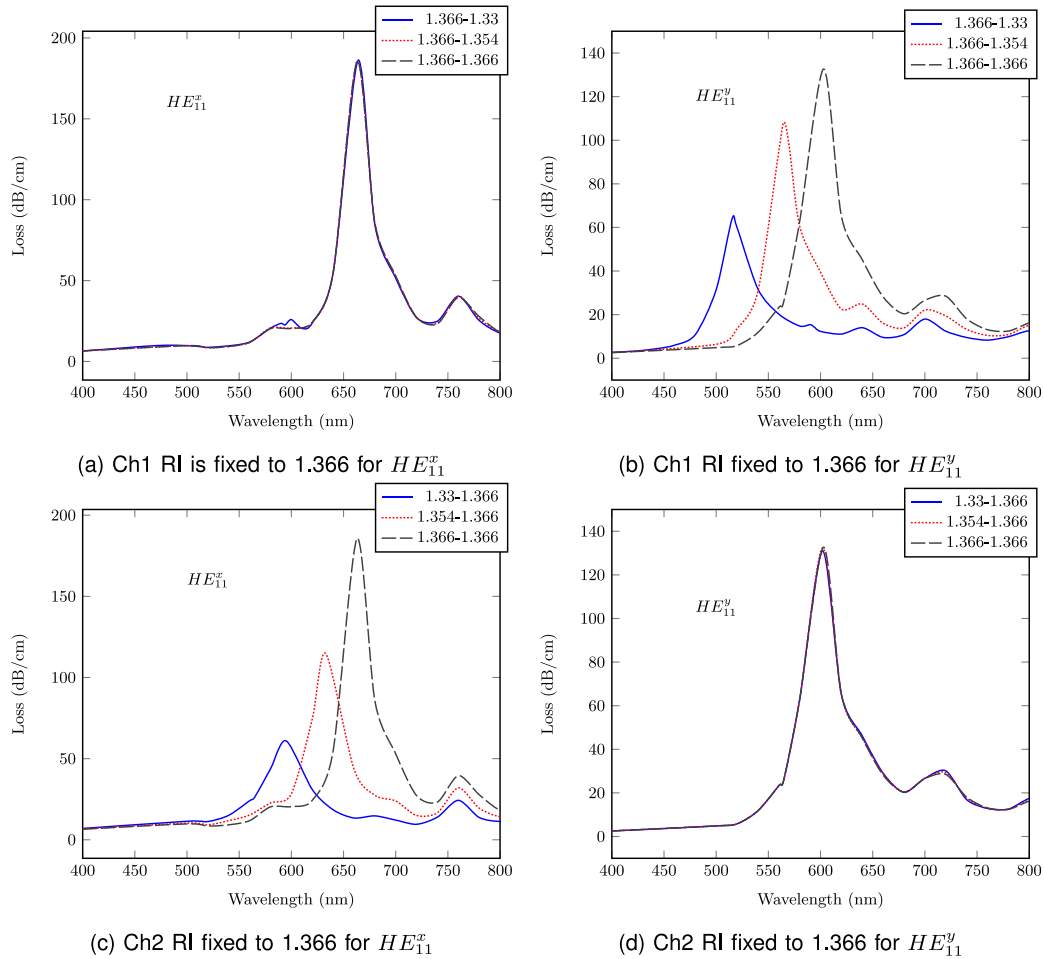(d) Ch2 RI fixed to 1.366 for HE_{11}^y

Fig. 6. Loss variation as a function of wavelength (RI fixed to 1.366) for both Channel 1 and 2.

The spectral sensitivity of the proposed sensor is summarized in Table 1. Numerical results presented in Fig. 3 to Fig. 6 are considered thoroughly. According to the loss characteristics of each graph, sensitivity results are calculated for both x- and y- polarized fundamental modes. It can be realized from the obtained results that y- mode becomes active whereas the x- mode becomes passive when the analyte RI is constant in Ch1. On the other hand, the x-polarized mode becomes active whereas y- mode becomes passive, where the analyte RI in Ch2 is kept constant. According to our simulation results, the highest spectral sensitivity is calculated as 2500 nm/RIU and 3083 nm/RIU with resolutions 4 x 10^{-5} RIU and 3.2 x 10^{-5} RIU, for x and y- polarized fundamental modes, respectively. Finally, the average sensitivities are obtained from the linear fitting calculations as 1892 nm/RIU and 2337 nm/RIU, for x and y- polarized modes, respectively. High Sensor linearity response is the desired parameter that determines the performance of the sensor applications. The linear fitting graph concerning the resonance wavelengths is presented in Fig. 10. The linear fitting equations for x- and y- polarized fundamental modes are given in Equations 4 and 5, respectively. The refractive index of an analyte is denoted by *n*. For different refractive index values, the average sensitivity is calculated from the slope of the following equations.

The linear response is calculated from the R^2, which is shown in Fig. 10. The proposed PCF sensor exhibits an excellent linear sensing response where high R^2 value indicates the high
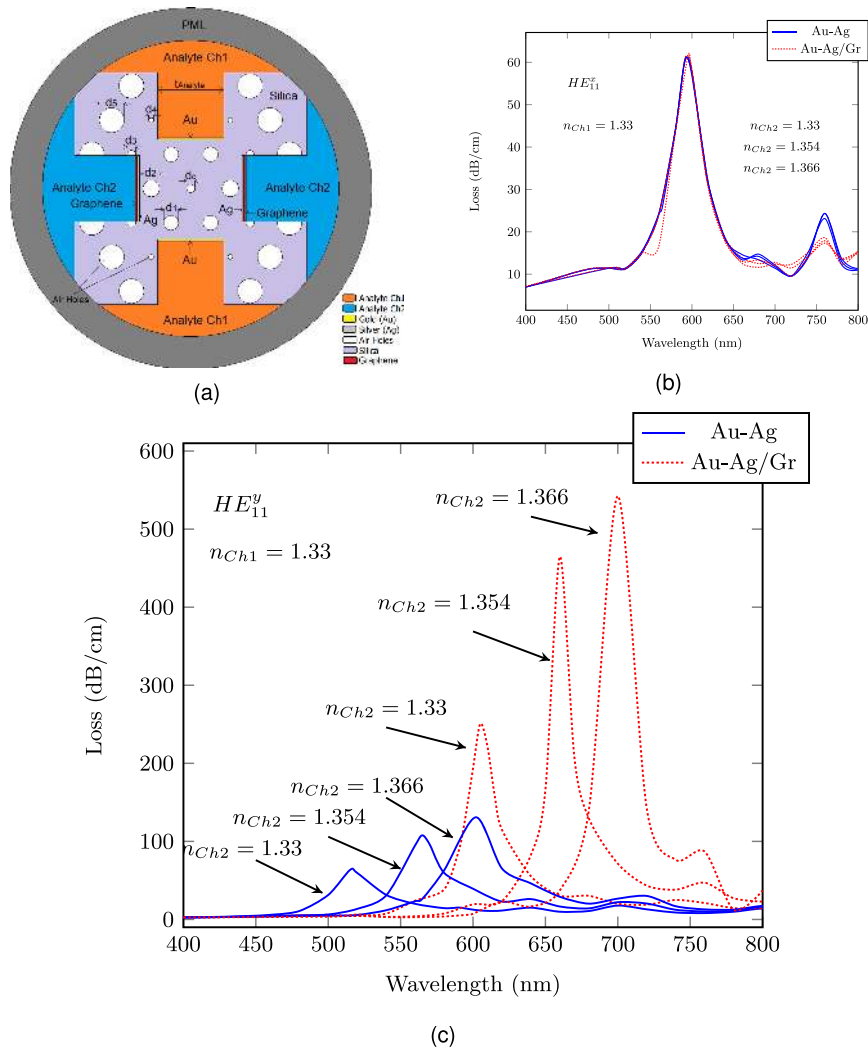
Fig. 7. Loss variation as a function of wavelength when graphene is used to protect silver and gold layers (when Ch1 RI is fixed to 1.33 and Ch2 RI is varied (1.33, 1.354 and 1.366)) (a) Cross section of graphene protected silver layer; (b) HE_{11}^x and (c) HE_{11}^y.

performance of the sensor design (as presented in Fig. 10).

$$\lambda_{HE_{11}^x} = 1892n - 1901, \quad 1.33 \leq n_a \leq 1.366 \tag{4}$$

$$\lambda_{HE_{11}^y} = 2337n - 2669, \quad 1.33 \leq n_a \leq 1.366 \tag{5}$$

The comparison of our proposed structure against previously published results has been presented in Table 2. Features such as the structural design, type of plasmonic material, wavelength, RI range, linearity and sensitivity parameters are considered for each reference sensor. It can be confirmed that the proposed sensor offers higher sensitivity when compared to the structures presented in Ref. [30], Ref. [32] and Ref. [33]. Although, results presented in Ref. [31] show that Ch1 exhibits higher sensitivity compared to our structure, Ch2 of our proposed structure demonstrates
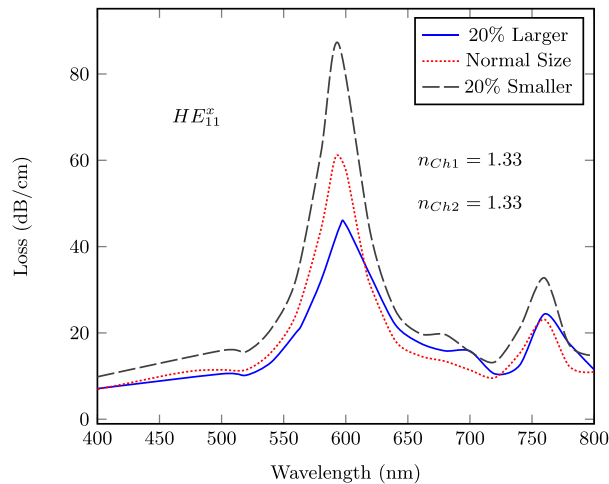
(a)
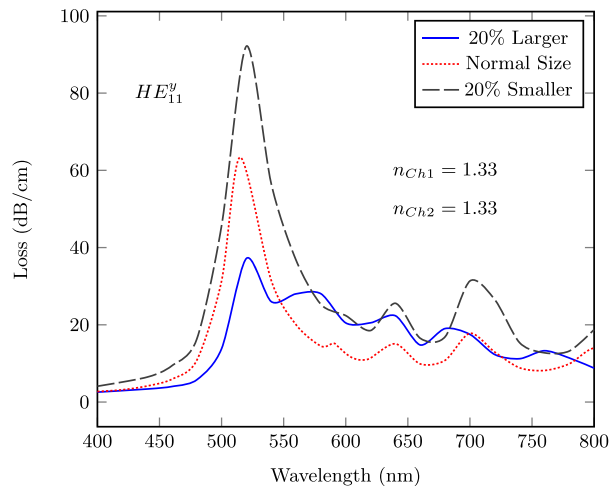
(b)

Fig. 8. The effect of air hole diameters d_1 and d_2 on loss curve (a) for HE_{11}^x and (b) for HE_{11}^y

better advanced sensitivity levels. It is worth pointing out that results in Ref. [34] are at a different wavelength range, therefore a true comparison is not possible.

Finally, conventional stack and draw or recently developed fused array preform method can be used for fabricating micron size air hole structures [40], [45]. Alternatively, the slurry casting [46] or sol-gel [47] methods which provides additional design flexibilities (independent adjustment of the hole size, shape, and spacing) can be used for fabricating cladding holes along the Ch1 and Ch2. The air holes can be organized precisely through careful process control. Therefore, the shift distance of cladding air holes, can be controlled efficiently [32]. Due to large analyte channels the analyte infiltration process will be easier. The analyte channels can be obtained by side-polishing technique [48]. Initially the structure can be etched from its edges with the height of t_{h1}, then from the middle of the etched section the etching process continue towards the centre of core with the width of t_w and the height of t_{h2}. The deposition of the metallic layers through the four analyte channels can be achieved by using High-pressure chemical vapour deposition or electroless plating techniques for Au layer [49], [50] and electron beam evaporation method for Silver layer [50]. It is
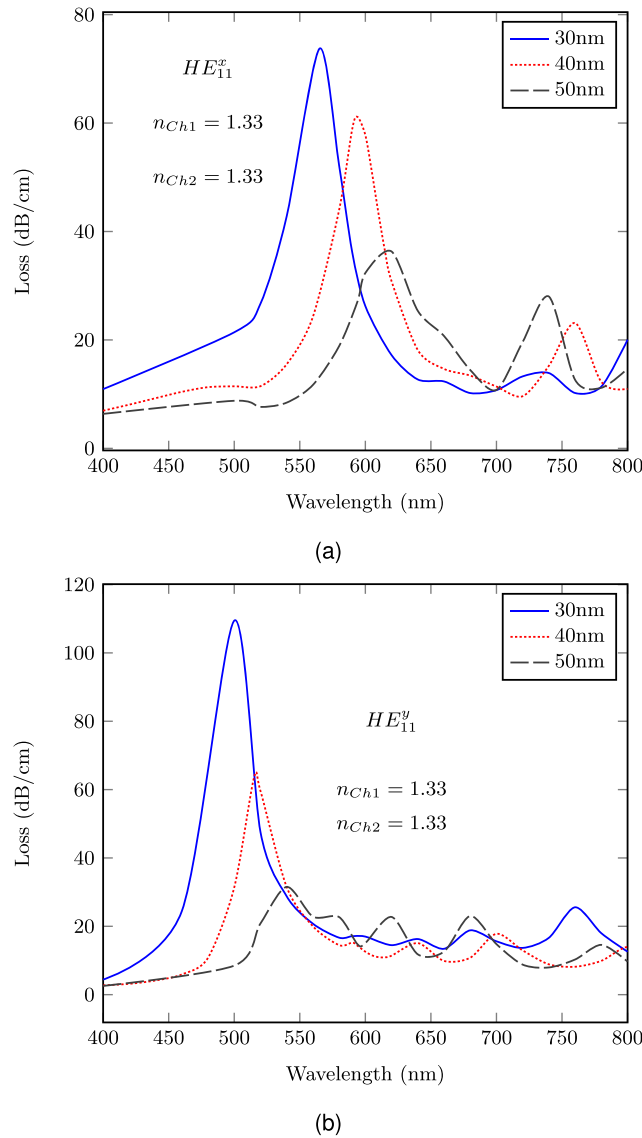
(a)

(b)

Fig. 9. The effect of metal layer thickness on loss levels (a) HE_{11}^x and (b) HE_{11}^y.

TABLE 1

SENSITIVITY AND RESOLUTION OUTCOMES OF PROPOSED SENSOR MODEL

	n_a	Sensitivity (nm/RIU)	Resolution (x10^{-5}RIU)	Average Sens. (nm/RIU)
x-polarized	1.33-1.354	1625	6.2	1892
	1.354-1.366	2500	4	
y-polarized	1.33-1.354	2083	4.8	2337
	1.354-1.366	3083	3.2	

worth noting that, the half shaped 8 cladding holes around the Ch2 may be filled with analyte during the etching process. Our numerical results have shown that, when half shaped cladding holes are filled with analyte, the performance of the proposed sensor will not be effected.

TABLE 2

PERFORMANCE COMPARISON OF PCF BASED SPR SENSORS FOR MULTI-ANALYTE SENSING

| Design	Plasmonic Material	Wavel. Range	RI Range	Sensitivity (nm/RIU)	Ref.
Three Channels	Au	500-800	1.36-1.46	1535 (Ch1) 1550 (Ch2)	[30]
Four Channels	Au/Ta_2TO_5	500-950	1.33-1.36	4600 (Ch1) 2300 (Ch2)	[31]
Four Channels	Au	600-680	1.33-1.34	2200 (Ch1) 2400 (Ch2)	[32]
Dual Channels	Ag/Au/ITO	400-1000	1.525-1.578	1951 (Ch1) 2496 (Ch2)	[33]
Two Analyte Ch.	Au	700-1100	1.3-1.40	1000 (Ch1) 3750 (Ch2)	[34]
Two Analyte Ch.	Au/Ag	400-800	1.33-1.366	2500 (Ch1) 3083 (Ch2)	This Work
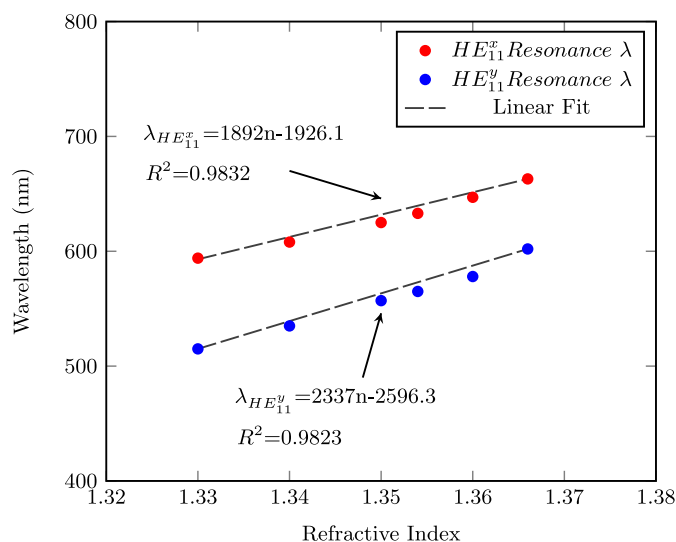
Fig. 10. Proposed sensor performance characteristics with respect to linear fitting equations.

4. Conclusion

In this study, a novel PCF based SPR sensor is proposed and demonstrated for multi-analyte sensing applications. Key sensor parameters such as; confinement losses, resonance conditions, metal layer thicknesses, air hole diameters, spectral sensitivities and their resolutions are investigated in terms of sensitivity and selectivity performance. The optimised SPR sensor achieved spectral sensitivity (RI between 1.33 and 1.366) up to 2500 nm/RIU and 3083 nm/RIU with 4×10^{-5} RIU and 3.2×10^{-5} RIU resolutions for Ch1 (x-polarized) and Ch2 (y-polarized), respectively. The demonstrated average sensitivities of the proposed sensor for both channels are; 1892 nm/RIU for Ch1 and 2337 nm/RIU for Ch2. Further, a high linearity for both channels, Ch1 and Ch2, has been obtained. It is demonstrated that the proposed SPR sensor design offers overall enhanced sensitivity performance compared to previously published multi-analyte studies [30]–[34].

Acknowledgment

References

[1] R. Jorgenson and S. Yee, "A fiber-optic chemical sensor based on surface plasmon resonance," *Sensors Actuators B: Chem.*, vol. 12, no. 3, pp. 213–220, 1993.

[2] C. Caucheteur, T. Guo, and J. Albert, "Review of plasmonic fiber optic biochemical sensors: Improving the limit of detection," *Analytical Bioanalytical Chem.*, vol. 407, no. 14, pp. 3883–3897, 2015.

[3] E. K. Akowuah, T. Gorman, H. Ademgil, S. Haxha, G. K. Robinson, and J. V. Oliver, "Numerical analysis of a photonic crystal fiber for biosensing applications," *IEEE J. Quantum Electron.*, vol. 48, no. 11, pp. 1403–1410, Nov. 2012.

[4] H. Chen *et al.*, "Label-free surface plasmon resonance cytosensor for breast cancer cell detection based on nano-conjugation of monodisperse magnetic nanoparticle and folic acid," *Sensors Actuators B: Chem.*, vol. 201, pp. 433–438, 2014.

[5] E. Kretschmann and H. Raether, "Radiative decay of non radiative surface plasmons excited by light," *Zeitschrift fur Naturforschung A¨*, vol. 23, no. 12, pp. 2135–2136, 1968.

[6] A. Hassani and M. Skorobogatiy, "Design of the microstructured optical fiber-based surface plasmon resonance sensors with enhanced microfluidics," *Opt. Exp.*, vol. 14, no. 24, pp. 11616–11621, 2006.

[7] M.-H. Chiu, C.-H. Shih, and M.-H. Chi, "Optimum sensitivity of single-mode D-type optical fiber sensor in the intensity measurement," *Sensors Actuators B: Chem.*, vol. 123, no. 2, pp. 1120–1124, 2007.

[8] R. K. Verma, A. K. Sharma, and B. Gupta, "Surface plasmon resonance based tapered fiber optic sensor with different taper profiles," *Opt. Commun.*, vol. 281, no. 6, pp. 1486–1491, 2008.

[9] S. Ge, F. Shi, G. Zhou, S. Liu, Z. Hou, and L. Peng, "U-shaped photonic crystal fiber based surface plasmon resonance sensors," *Plasmonics*, vol. 11, no. 5, pp. 1307–1312, 2016.

[10] L.-Y. Shao, Y. Shevchenko, and J. Albert, "Intrinsic temperature sensitivity of tilted fiber Bragg grating based surface plasmon resonance sensors," *Opt. Exp.*, vol. 18, no. 11, pp. 11464–11471, 2010.

[11] E. Popov, N. Bonod, and S. Enoch, "Comparison of plasmon surface waves on shallow and deep metallic 1D and 2D gratings," *Opt. Exp.*, vol. 15, no. 7, pp. 4224–4237, 2007.

[12] T. Huang, "Highly sensitive SPR sensor based on D-shaped photonic crystal fiber coated with indium tin oxide at near-infrared wavelength," *Plasmonics*, vol. 12, no. 3, pp. 583–588, 2017.

[13] W. C. Wong *et al.*, "Photonic crystal fiber surface plasmon resonance biosensor based on protein G immobilization," *IEEE J. Sel. Topics Quantum Electron.*, vol. 19, no. 3, May/Jun. 2013, Art. no. 4602107.

[14] A. Yasli and H. Ademgil, "Effect of plasmonic materials on photonic crystal fiber based surface plasmon resonance sensors," *Modern Phys. Lett. B*, vol. 33, no. 13, 2019, Art. no. 1950157.

[15] Q. Liu, B. Yan, and J. Liu, "U-shaped photonic quasi-crystal fiber sensor with high sensitivity based on surface plasmon resonance," *Appl. Phys. Exp.*, vol. 12, no. 5, 2019, Art. no. 052014.

[16] S. Chu, K. Nakkeeran, A. M. Abobaker, S. S. Aphale, P. R. Babu, and K. Senthilnathan, "Design and analysis of surface-plasmon-resonance-based photonic quasi-crystal fiber biosensor for high-refractive-index liquid analytes," *IEEE J. Sel. Topics Quantum Electron.*, vol. 25, no. 2, Mar./Apr. 2019, Art. no. 6900309.

[17] C. Li, B. Yan, and J. Liu, "Refractive index sensing characteristics in a D-shaped photonic quasi-crystal fiber sensor based on surface plasmon resonance," *JOSA A*, vol. 36, no. 10, pp. 1663–1668, 2019.

[18] B. Yan *et al.*, "Polarization filtering in the visible wavelength range using surface plasmon resonance and a sunflower-type photonic quasicrystal fiber," *J. Phys. D: Appl. Phys.*, vol. 51, no. 15, 2018, Art. no. 155105.

[19] E. Liu, W. Tan, B. Yan, J. Xie, R. Ge, and J. Liu, "Broadband ultra-flattened dispersion, ultralow confinement loss and large effective mode area in an octagonal photonic quasi-crystal fiber," *JOSA A*, vol. 35, no. 3, pp. 431–436, 2018.

[20] E. Liu, B. Yan, W. Tan, J. Xie, R. Ge, and J. Liu, "Guiding characteristics of sunflower-type fiber," *Superlattices Microstructures*, vol. 115, pp. 123–129, 2018.

[21] J. Han, E. Liu, and J. Liu, "Circular gradient-diameter photonic crystal fiber with large mode area and low bending loss," *JOSA A*, vol. 36, no. 4, pp. 533–539, 2019.

[22] E. Liu, S. Liang, and J. Liu, "Double-cladding structure dependence of guiding characteristics in six-fold symmetric photonic quasi-crystal fiber," *Superlattices Microstructures*, vol. 130, pp. 61–67, 2019.

[23] Y. Cai *et al.*, "Properties of defect modes in two-dimensional organic octagonal quasicrystals at low dielectric contrast," *Opt. Commun.*, vol. 427, pp. 6–12, 2018.

[24] S. Zhang, X. Yu, P. Shum, Y. Zhang, H. Ho, and D. Liu, "Highly sensitive pressure-induced plasmon resonance birefringence in a silver-coated photonic crystal fiber," in *Proc. J. Phys.: Conf. Ser.*, 2011, vol. 276, Art. no. 012102.

[25] Y. S. Lee, C. G. Lee, and S. Kim, "Annular core photonic quasi-crystal fiber with wideband nearly zero ultra-flat dispersion, low confinement loss and high nonlinearity," *Optik*, vol. 157, pp. 141–147, 2018.

[26] W. Wei *et al.*, "Refractive index sensors based on Ag-metalized nanolayer in microstructured optical fibers," *Optik-Int. J. Light Electron. Opt.*, vol. 123, no. 13, pp. 1167–1170, 2012.

[27] J. N. Dash and R. Jha, "On the performance of graphene-based D-shaped photonic crystal fibre biosensor using surface plasmon resonance," *Plasmonics*, vol. 10, no. 5, pp. 1123–1131, 2015.

[28] A. A. Rifat *et al.*, "Copper-graphene-based photonic crystal fiber plasmonic biosensor," *IEEE Photon. J.*, vol. 8, no. 1, Feb. 2016, Art. no. 4800408.

[29] A. Yasli and H. Ademgil, "Geometrical comparison of photonic crystal fiber-based surface plasmon resonance sensors," *Opt. Eng.*, vol. 57, no. 3, 2018, Art. no. 030801.

[30] Y. Zhang, C. Zhou, L. Xia, X. Yu, and D. Liu, "Wagon wheel fiber based multichannel plasmonic sensor," *Opt. Exp.*, vol. 19, no. 23, pp. 22863–22873, 2011.

[31] R. Otupiri, E. K. Akowuah, and S. Haxha, "Multi-channel SPR biosensor based on PCF for multi-analyte sensing applications," *Opt. Exp.*, vol. 23, no. 12, pp. 15716–15727, 2015.

[32] S. I. Azzam, M. F. O. Hameed, R. E. A. Shehata, A. Heikal, and S. S. Obayya, "Multichannel photonic crystal fiber surface plasmon resonance based sensor," *Opt. Quantum Electron.*, vol. 48, no. 2, 2016, Art. no. 142.

[33] M. Lu *et al.*, "Dual channel multilayercoated surface plasmon resonance sensor for dual refractive index range measurements," *Opt. Exp.*, vol. 25, no. 8, pp. 8563–8570, 2017.

[34] V. Kaur and S. Singh, "A dual-channel surface plasmon resonance biosensor based on a photonic crystal fiber for multianalyte sensing," *J. Comput. Electron.*, vol. 18, no. 1, pp. 319–328, 2019.

[35] R. Kamikawachi *et al.*, "Determination of thermo-optic coefficient in liquids with fiber Bragg grating refractometer," *Opt. Commun.*, vol. 281, no. 4, pp. 621–625, 2008.

[36] A. K. Sharma, R. Jha, and B. Gupta, "Fiber-optic sensors based on surface plasmon resonance: A comprehensive review," *IEEE Sensors J.*, vol. 7, no. 8, pp. 1118–1129, Aug. 2007.

[37] H. Philipp and E. D. Palik, *Handbook of Optical Constants of Solids*, vol. 749, Palik, Ed. Orlando, FL, USA: Academic, 1985, p. 74.

[38] C. Liu *et al.*, "Numerical analysis of a photonic crystal fiber based on a surface plasmon resonance sensor with an annular analyte channel," *Opt. Commun.*, vol. 382, pp. 162–166, 2017.

[39] C. Hao, Y. Lu, M. Wang, B. Wu, L. Duan, and J. Yao, "Surface plasmon resonance refractive index sensor based on active photonic crystal fiber," *IEEE Photon. J.*, vol. 5, no. 6, Dec. 2013, Art. no. 4801108.

[40] A. Rifat *et al.*, "Surface plasmon resonance photonic crystal fiber biosensor: A practical sensing approach," *IEEE Photon. Technol. Lett.*, vol. 27, no. 15, pp. 1628–1631, Aug. 2015.

[41] E. Klantsataya, P. Jia, H. Ebendorff-Heidepriem, T. M. Monro, and A. François, "Plasmonic fiber optic refractometric sensors: From conventional architectures to recent design trends," *Sensors*, vol. 17, no. 1, 2016, Art. no. 12.

[42] J. N. Dash and R. Jha, "Graphene-based birefringent photonic crystal fiber sensor using surface plasmon resonance," *IEEE Photon. Technol. Lett.*, vol. 26, no. 11, pp. 1092–1095, Jun. 2014.

[43] E. Akowuah, T. Gorman, H. Ademgil, and S. Haxha, "A highly sensitive photonic crystal fibre (PCF) surface plasmon resonance (SPR) sensor based on a bimetallic structure of gold and silver," in *Proc. IEEE 4th Int. Conf. Adaptive Sci. Technol.*, 2012, pp. 121–125.

[44] M. F. O. Hameed, Y. K. Alrayk, A. A. Shaalan, W. S. El Deeb, and S. S. Obayya, "Design of highly sensitive multichannel bimetallic photonic crystal fiber biosensor," *J. Nanophoton.*, vol. 10, no. 4, 2016, Art. no. 046016.

[45] P. Falkenstein and B. L. Justus, "Fused array preform fabrication of holey optical fibers," U.S. Patent 8 433 167, Apr. 30, 2013.

[46] T. Yajima, J. Yamamoto, F. Ishii, T. Hirooka, M. Yoshida, and M. Nakazawa, "Low-loss photonic crystal fiber fabricated by a slurry casting method," *Opt. Exp.*, vol. 21, no. 25, pp. 30500–30506, 2013.

[47] R. T. Bise and D. Trevor, "Solgel-derived microstructured fibers: Fabrication and characterization," in *Proc. Opt. Fiber Commun. Conf.*, 2005, Art. no. OWL6.

[48] H. Kim, J. Kim, U.-C. Paek, B. H. Lee, and K. T. Kim, "Tunable photonic crystal fiber coupler based on a side-polishing technique," *Opt. Lett.*, vol. 29, no. 11, pp. 1194–1196, 2004.

[49] N. Takeyasu, T. Tanaka, and S. Kawata, "Metal deposition deep into microstructure by electroless plating," *Jpn. J. Appl. Phys.*, vol. 44, no. 8L, pp. L1134–L 1137, 2005.

[50] J. A. Harrington, "A review of IR transmitting, hollow waveguides," *Fiber Integr. Opt.*, vol. 19, no. 3, pp. 211–227, 2000.